Journal of
10/15
BIOPHOTONICS
www.biophotonics-journal.org

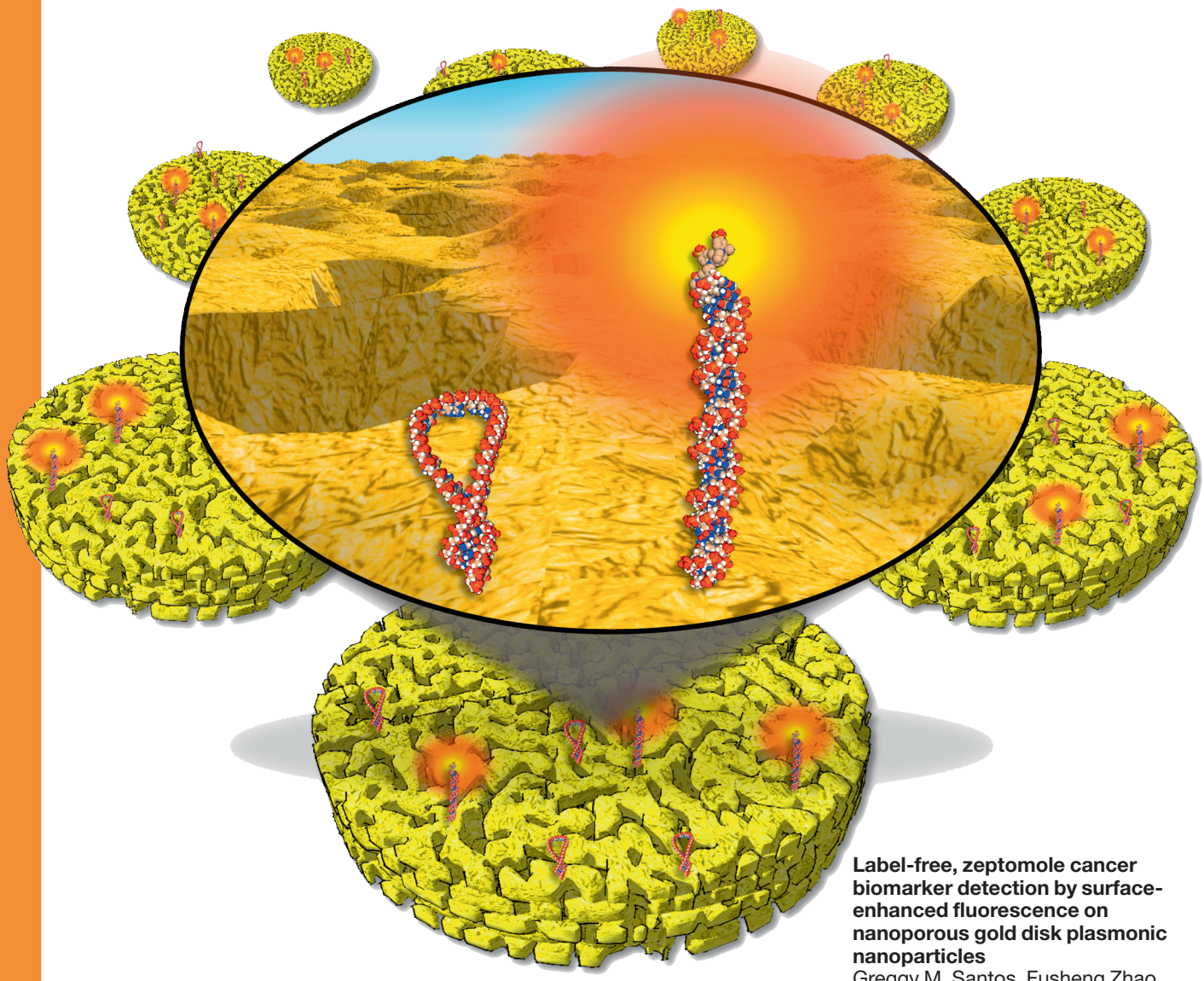

Label-free, zeptomole cancer biomarker detection by surface-enhanced fluorescence on nanoporous gold disk plasmonic nanoparticles
Greggy M. Santos, Fusheng Zhao, Jianbo Zeng, Ming Li, Wei-Chuan Shih

WILEY-VCH
ISSN 1864-0648 J. Biophotonics, Vol. **8**, No. 10 (October), 775–863 (2015)

J. Biophotonics **8**, No. 10, 855–863 (2015) / **DOI** 10.1002/jbio.201400134

Journal of BIOPHOTONICS

FULL ARTICLE

Label-free, zeptomole cancer biomarker detection by surface-enhanced fluorescence on nanoporous gold disk plasmonic nanoparticles

*Greggy M. Santos, Fusheng Zhao, Jianbo Zeng, Ming Li, and Wei-Chuan Shih**

Department of Electrical and Computer Engineering, University of Houston, 4800 Calhoun Road, Houston, Texas 77204, USA

Received 10 November 2014, revised 22 January 2015, accepted 5 February 2015
Published online 24 February 2015

Key words: surface-enhanced fluorescence, nanoporous gold disks, label-free biosensor, zeptomole detection, molecular beacon

We experimentally demonstrate a label-free biosensor for the ERBB2 cancer gene DNA target based on the distance-dependent detection of surface-enhanced fluorescence (SEF) on nanoporous gold disk (NPGD) plasmonic nanoparticles. We achieve detection of 2.4 zeptomole of DNA target on the NPGD substrate with an upper concentration detection limit of 1 nM. Without the use of molecular spacers, the NPGD substrate as an SEF platform was shown to provide higher net fluorescence for visible and NIR fluorophores compared to glass and non-porous gold substrates. The enhanced fluorescence signals in patterned nanoporous gold nanoparticles make NPGD a viable material for further reducing detection limits for biomolecular targets used in clinical assays.

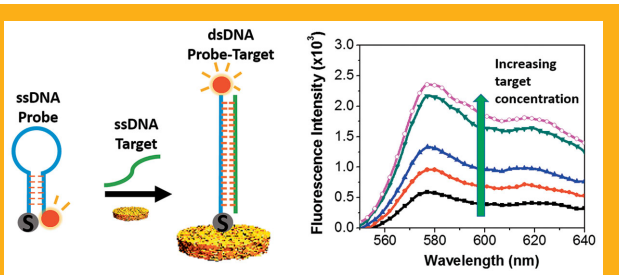

With patterned nanoporous gold disk (NPGD) plasmonic nanoparticles, a label-free biosensor that makes use of distance-dependent detection of surface-enhanced fluorescence (SEF) is constructed and tested for zeptomole detection of ERBB2 cancer gene DNA targets.

1. Introduction

Fluorescence measurements have been indispensable in probing specific biological and biochemical processes. Challenges in improving signal intensity resulted to heightened interest in techniques that enhance fluorescence signals. By modifying the spontaneous emission via resonant coupling with an external electric field, several techniques have been developed to modulate fluorescence intensity including the use of controlled electron transfer [1–2], resonant cavities [3–4], quantum wells [5], and photonic crystals [6–7]. Surface-enhanced fluorescence (SEF), known also as metal-enhanced fluorescence (MEF), has attracted attention for its potential in fluorescence enhancement [8–11]. SEF occurs when fluorophores are within nanoscale proximity from surfaces of metallic nanostructures. Through the use of specifically designed metal nanostructures, increased fluorescence enhancement factors up to 500 times has been reported [12]. More typically, enhancement in the range of 5–50 times has been observed [8, 10, 13–14]. Even with less enhancement, the SEF process has been proven to be advanta-

* Corresponding author: e-mail: wshih@uh.edu

© 2015 by WILEY-VCH Verlag GmbH & Co. KGaA, Weinheim

geous from various aspects: faster spontaneous emission processes, increased quantum yields, improved fluorophore photostability, and shortened fluorescent lifetime [15–16]. SEF studies have gained attention in the chemical and biological research community due to these potential benefits.

In SEF, the metallic nanostructure assumes a more active role in enhancing the fluorescence signal compared to conventional dielectric substrates. However, a critical issue of SEF is its compatibility for practical technologies used in biosensing and bioimaging. Hence, it is of prime importance to explore new materials that increases the utility of SEF in relevant applications.

Due to its 3-dimensional nanoscale architecture, nanoporous gold (NPG) has become a versatile nanomaterial [17–20]. Being plasmonic, NPG thin film provides a potentially useful platform for fluorescence enhancement in chemical and biological studies. It has been demonstrated that the localized surface plasmon resonance (LSPR) of thin-film NPG materials are related to its pore size [20–21]. Hence, the SEF properties of NPG thin films can be tuned, to a certain degree, by altering the morphology of the nanoporous network (pore and ligament size). NPG can be understood as a network of small nanoparticles that synergistically provide coupled field enhancement. The plasmonic coupling within adjacent pores and connecting ligaments result in points with high concentration of electromagnetic field known as "hot spots" [18, 21–22].

Recently, we have demonstrated that patterned NPG nanoparticles in disk shape are excellent plasmonic nanomaterials with tunable plasmonics, 3-dimensional plasmonic hot spot distribution, large surface area, and large surface-enhanced Raman scattering (SERS) enhancement factor [22–25]. The plasmon resonance associated with the disk shape promotes effective light coupling and generates higher field enhancement compared to that in NPG thin films. Taking advantage of the high-density hot spots in nanoporous gold disks (NPGDs), we have developed several applications such as photothermal conversion and light-gated molecular delivery [26], ultrasensitive DNA hybridization monitoring at the level of individual molecules [27], label-free molecular sensing and imaging by stamping NPGD substrate onto a flexible surface with target analytes [28], and integrated microfluidic SERS sensor for label-free biomolecular sensing [29]. There has been no report regarding SEF on patterned NPG nanoparticles.

When fluorophores are near metal surfaces, electronic energy transfer from the molecule may occur which generally leads to fluorescence quenching [30]. Therefore, the fluorescence measured on "naked" metallic substrates is typically the outcome of the competition between SEF and metal-induced quenching. From past studies, quenching is known to be the dominant effect for nanoparticle-fluorophore distances smaller than ~5 nm, whereas enhancement has been reported mostly for distances between ~5 nm and 20 nm [14, 30–31]. Based on these results, most existing SEF demonstrations, including those on thin-film NPG materials, involved spacers to place fluorophores at the "sweet spot" [32–33]. Using a protein spacer, Lang et al. investigated the enhanced Indocyanine Green (ICG) fluorescence on NPG thin films with pore structures of different characteristic lengths [33].

In this paper, we present a label-free DNA hybridization sensor on NPGDs. Our design strategy is to utilize the distance-dependent enhancing and quenching mechanisms to our advantage and to effectively circumvent the need of additional spacers. We have adopted a distance-modulation scheme based on DNA hybridization commonly employed in molecular beacon. Using a "hairpin" single-stranded DNA (ssDNA) probe featuring a Cyanine 3 (Cy3) fluorophore on the 3′-end and a sulfur on the 5′-end, the distance between the Cy3 molecule and NPGD can be altered. By taking advantage of the distance modulation, the sensitivity of the NPGD sensor to target DNA with 28 complementary base pairs is demonstrated. Detection of short DNA target sequences (<30 base pairs) is suitably relevant to applications in micro-RNA detection for early stage cancer diagnosis [34–36]. To characterize the interplay of enhancing and quenching on NPGDs, we have compared three fluorophores on three different gold substrates. These results provide the foundation for sensor design and characterization.

2. Methods

2.1 Chemicals, materials, and NPGD fabrication

Mercapto-1-hexanol (MCH), Rhodamine 6G (R6G), Cyanine 3 (Cy3) were purchased from Sigma-Aldrich. The IRDye 800 infrared dye was purchased from Licor Biosciences. The ssDNA probe and target molecules were purchased from Integrated DNA Technologies (IDT, Coralville, IA). The NPG disks (400 nm in diameter, 75 nm thickness, and 13 nm average pore size) and non-porous gold disks were fabricated according to methods in recent studies published [22–23]. The fabrication of substrate-bound NPGD arrays initiates with sputtering a 120 nm thick film of Au : Ag (30 : 70) alloy over the glass coverslip (~165 μm thick) by DC sputtering. A monolayer of 600 nm polystyrene (PS) beads were then deposited on the surface of the alloy film. To shrink and isolate each PS bead, oxygen plasma-etching was employed,

© 2015 by WILEY-VCH Verlag GmbH & Co. KGaA, Weinheim

Table 1 ERBB2 probe and target sequences.

ssDNA	DNA sequence
ERBB2 probe	5′-SH-*CGCCAT*CCACCCCCAAGACCACGACCAGCAGAAT*ATGGCG*-Cy3-3′
ERBB2 target	5′-GTTGGCATTCTGCTGGTCGTGGTCTTGGGGGTGGTCTTTG-3′

followed by Ar plasma-etching to induce alloy disk formation on the glass surface. The remaining PS beads were removed by sonication in chloroform which leaves only the alloy disk pattern on the glass coverslip. The disks were dealloyed in 70% nitric acid for 1 minute followed by DI water wash for 2 minutes. The surface morphology and monolayer coverage of NGPDs on glass are shown in SEM images found in Figure S1 of Supporting Information. Colloidal NPGD particles were prepared by sonicating off the nanoparticles from the glass coverslip for 30 mins in 100 μM R6G aqueous solution. The R6G-loaded colloidal NPGD was then centrifuged from the dye solution and resuspended in DI water.

2.2 DNA probe and target molecules

We employed a hairpin probe sequence complementary to the ERBB2 oncogene, a target breast cancer DNA biomarker. Table 1 shows the sequences of the probe and target. The italicized portion shows the complementary sequence that forms the "stem" in the hairpin probe structure while the underlined portion shows the complementary sequence for the probe-target pair.

2.3 Fluorescence and extinction measurements

Fluorescence emission spectra were acquired using home-built inverted fluorescence microscopy systems with 532 nm and 785 nm CW laser sources, dispersive spectrographs and thermoelectrically (TE) cooled charged coupled device (CCD) cameras as detector [37–39]. The acquisition time used varied from 10 to 30 seconds at a laser power density of 0.5 W/cm^2. The laser power density level used for the study is comparable to values in existing SEF studies [3, 40]. With a laser spot size of 1.77 μm^2, we measured sample regions of uniform disk coverage (~7 disks per laser spot) to ensure repeatability of total fluorescence measurements (see Figure S1). A Jasco V-570 spectrometer was used to measure the UV-Vis-NIR extinction spectra (400–1500 nm) of the NPGD and non-porous gold disk arrays on glass. The extinction spectra were collected at 0° normal incidence.

3. Results and discussion

3.1 Fluorescence enhancement on NPGD substrates at different dye concentrations

Here we investigate fluorescence enhancement on the NPGD substrate at different dye concentrations. Figure 1A shows the fluorescence spectra acquired from various Rhodamine 6G (R6G) concentrations on NPGD substrates normalized to those from glass substrates. The data acquisition and experimental protocols can be found in Methods. Details of NPGD substrate fabrication are provided in Methods. Using the peak intensity at 565 nm, the relative fluorescence intensity from each concentration are displayed in Figure 1B by normalizing to the peak intensity from the glass substrates. We observe a net gain up to 50 times for higher concentrations (1 μM and 100 nM), but a net loss for lower concen-

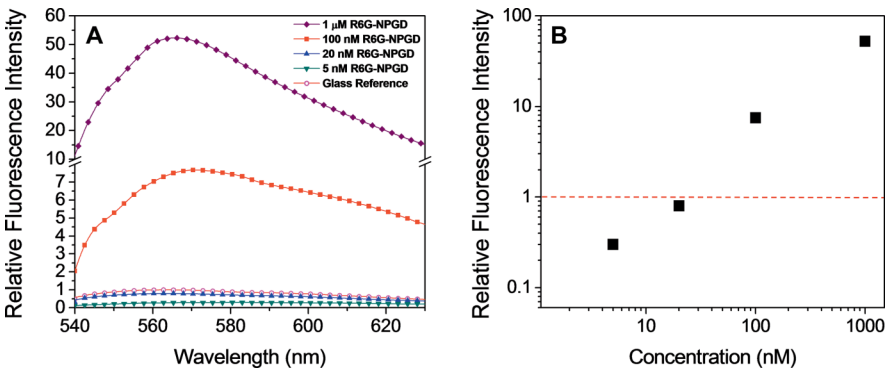

Figure 1 Concentration dependence of R6G fluorescence: (**A**) Normalized spectra from various concentrations on NPGD substrates compared to glass substrates; (**B**) Relative fluorescence intensity on NPGD substrates. The aqueous dye solution (volume: 5 μL; concentration: 5 nM to 1 μM) was dropcasted on all substrates.

© 2015 by WILEY-VCH Verlag GmbH & Co. KGaA, Weinheim

trations (20 nM and 5 nM). We note that this value (50 times) should not be interpreted as the typically reported enhancement factor because no spacer was employed in our experiments. In other words, the total fluorescence signals were the outcome of combined quenching and enhancement effects. Thus, the actual SEF enhancement factor can be higher.

The total fluorescence intensity is likely affected by the average surface density of the adsorbed dye molecules, which is directly related to solution concentrations. At higher concentrations (~1 μM), molecules have a higher probability to "pile up" on top of the metal surface, where the molecules in direct contact with metal become effective "spacers" for those farther away from the surface. As the surface density decreases, a larger fraction of molecules are in direct contact with the metal and more likely to suffer quenching rather than enhancement. For an adsorbed R6G molecule occupying an area of ~20 Å^2, the monolayer coverage for a flat surface is about 5 million molecules per μm^2 [41–42]. In our experiment, the dried spot size was ~3 mm in diameter, resulting in an average surface density of ~42,500 molecules per μm^2 for the 100 nM sample. This suggests that considerable enhancement still contributed the nearly 10 times total fluorescence even at sub-monolayer coverage, likely due to the high-density hot spots in NPGDs. This is in contrast to nearly negligible enhancement on a flat gold film substrate as discussed later.

3.2 *Fluorescence enhancement comparison on various fluorophores and substrates*

To characterize the fluorescence enhancement properties of NPGDs, fluorescence emission spectra were collected from three dyes on three different gold substrates. In each experiment, a 5 μL drop of 100 nM dye solution was dispensed and dried on the substrate. Figure 2 shows the fluorescence spectra of the dyes (Rhodamine 6G (R6G), Cyanine 3 (Cy3), and IRDye 800) on four different substrates (NPGD, non-porous gold disks, flat gold film, and a glass substrate). The NPGDs were of 400 nm diameter, 75 nm thickness, and 13 nm average pore size. The non-porous gold disks were of the same external size. The flat gold film was 75 nm in thickness. R6G (526/560 nm) and Cy3 (550/570 nm) absorb and emit strongly in the visible region while IRDye 800 (780/800 nm) in the near infrared (NIR). All fluorescence spectra were normalized to the peak value of the one obtained from the glass substrate. In other words, the glass substrate was used as a reference to compare the total fluorescence from various gold substrates.

As shown in Figure 2, NPGD substrates exhibited the strongest total fluorescence for all three dyes, as compared to the other gold substrates (gold disk and gold film). The net gain obtained on NPGD substrates were ~7, 7, and 1.75 times compared to the glass substrate for R6G, Cy3, and IRDye 800, respectively. The flat gold substrate provided the lowest fluorescence with net gain slightly larger than 1 for R6G and Cy3, and ~0.6 for IRDye, suggesting quenching dominated over enhancement. The non-porous gold disks provided medium fluorescence with net gain ~3–4 times for R6G and Cy3, and 1.15 times for IRDye.

The larger net gain on NPGDs is attributed to higher field enhancement within the high-density plasmonic hot-spots, which are unique features only seen in NPGDs. It is interesting to compare the extinction spectra of NPGD and non-porous gold disk as shown in Figure 3. The LSPR peak for non-porous gold disk and NPGD are at 800 nm and 1050 nm, respectively, indicating that the LSPR peak for the non-porous Au disks is closer to the excitation/emission wavelengths for either the visible or NIR dye. Typically, higher plasmonic enhancement can be obtained when the excitation/emission wavelengths are

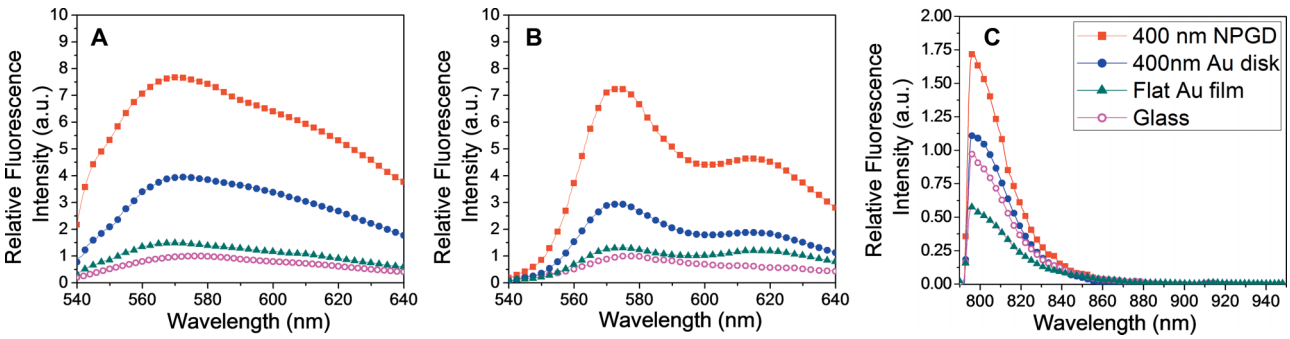

Figure 2 Comparison of fluorescence spectra from 3 dyes on 4 substrates: (**A**) R6G and (**B**) Cy3 dyes dried on NPGD and gold disk samples acquired using a home-built fluorescence microscope with 532 nm excitation, (**C**) IRDye 800 dye fluorescence measured using a home-built fluorescence microscope with 785 nm excitation. An amount of 5 μL of the 100 nM aqueous dye solutions was dropcasted on each substrate.

© 2015 by WILEY-VCH Verlag GmbH & Co. KGaA, Weinheim

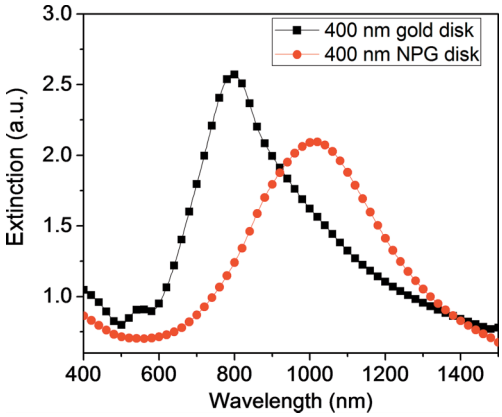

Figure 3 Extinction spectra of non-porous gold disks (400 nm diameter) and NPGDs (400 nm diameter).

better aligned with the substrate LSPR [13]. In addition, dyes with lower quantum yields (i.e. NIR dyes) are known to exhibit larger fluorescence enhancement [43–44]. However, we note that the measurements reported in Figures 1 and 2 are the total fluorescence intensities, and not the actual SEF which is more dependent on dye quantum yield and band overlap. Nevertheless, NPGD still exhibited stronger total fluorescence. In future studies, the performance of NPGDs would be further improved by employing disks with smaller diameters, which exhibit blue-shifted plasmon peak as revealed in our previous studies [22, 24].

3.3 Fluorescence imaging of NPGDs

Next we investigate the spatial distribution of R6G fluorescence enhancement effect on NPGDs. The brightfield image in Figure 4A provides location information of individual NPGDs, and the fluorescence image in Figure 4B provides the corresponding R6G fluorescence intensity. It is observed that brighter pixels are significantly localized near NPGDs, suggesting that the enhancement was indeed a near-field effect of LSPR.

As reported in our previous paper, colloidal NPGDs can be obtained by sonication [22]. Fluorophore-loaded colloidal NPGDs can be alternatively employed as a high brightness fluorescence label. In Figure 4C, colloidal NPGD particles were preloaded with R6G dye molecules through incubation with details described in Methods. The particles were then centrifuged, collected and dropcasted on a glass substrate. The nanoporous network of NPGDs has been shown to carry a larger amount of molecules compared to non-porous gold substrates [26]. At the same time, the abundance of enhancement sites found in nanoporous surfaces results in enhanced fluorescent signals from the harbored dyes. NPGDs can be loaded with a flexible range of fluorophore amounts to achieve desired fluorescent levels. NPGDs is not only a potentially versatile fluorescent label but also effective molecular cargo for light-gated release through photothermal mechanisms [26].

3.4 Zeptomole detection of cancer DNA biomarker

NPGD can be employed as a DNA sensor based on hybridization, where two single-stranded DNA (ssDNA) molecules form a duplex through non-covalent, sequence-specific interactions, a fundamental process in biology [45]. Developing a better understanding of the kinetics and dynamic aspects of hybridization will help reveal molecular mechanisms involved in numerous biomolecular processes. To this end, hybridization sensor has been instrumental and a ubiquitous tool in a wide variety of biological and biomedical applications such as clinical diagnostics, biosensors, and drug development [46]. Label-free and amplification-free schemes are of particular interest because they could potentially provide *in situ* monitoring of individual hybridization events, which may lead to techniques for discriminating subtle variations due to single-base modification without stringency control or repetitive thermal cycling. Unlike most fluorescence techniques, molecu-

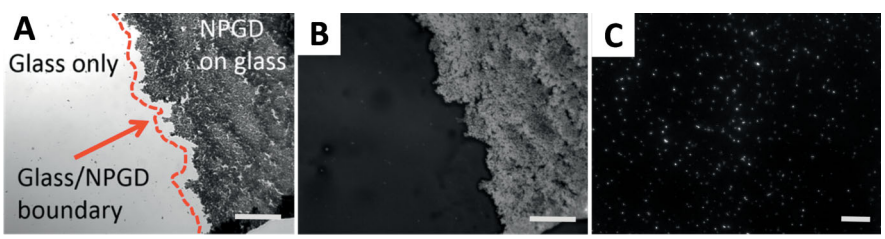

Figure 4 Brightfield and fluorescence images (20×) of 400 nm NPGD substrate with adsorbed R6G (1 μM): (**A**) brightfield with boundary between glass-only and NPGD regions shown by the dashed curve, and (**B**) fluorescence image. (**C**) Fluorescence images (40×) of NPGD (400 nm diameter) preloaded with R6G and dropcasted and dried on glass from colloidal suspension. Scale bar is 20 μm.

© 2015 by WILEY-VCH Verlag GmbH & Co. KGaA, Weinheim

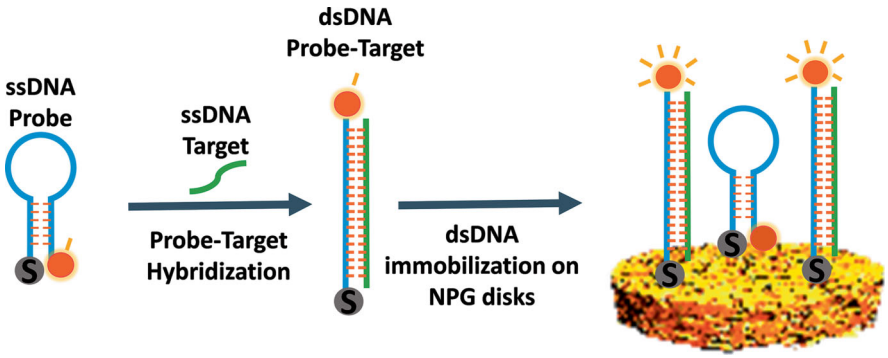

Figure 5 Schematic of the hairpin probe and probe-target (dsDNA) configurations of the ERBB2 cancer gene, and their immobilization on NPGDs.

lar beacons (MB) provide label-free detection. Recently, a reporting mechanism similar to MB probes has been implemented by Peng et al. on 15 nm colloidal silver nanoparticles to harness surface-enhanced fluorescence and achieved a limit of detection (LOD) of ~500 pM for the *Bacillus Anthracis* bacterial gene target [47].

Here a "hairpin" ssDNA probe is employed to detect ERBB2 breast cancer biomarker. The probe features a Cy3 on the 3′-end and a sulfur on the 5′-end that enables effective binding to gold surfaces. If the probe alone is bonded, the Cy3 molecule is positioned at the close proximity of the NPGD surface, which promotes quenching. In contrast, a hybridized ds-DNA would have the Cy3 molecule on the opposite end of the sulfur and far away from the NPGD surface after binding (see Figure 5). Such conformation induced modulation of plasmonic enhancement has been employed in our previous work based on surface-enhanced Raman scattering (SERS) technique [27]. The detailed ssDNA sequence information are provided in the Methods. As compared to the un-hybridized hairpin probe on NPGD, higher fluorescence intensity is expected for the ds-DNA configuration, providing an effective sensing mechanism.

In the previous dropcasting method, the likelihood for the fluorophore molecules to be situated in the enhancing hot spots of the NPGD is highly dependent on the local dye-NPGD molecular interactions and dye concentration. In contrast, due to its inherent self-assembly mechanism and robust sulfur-gold covalent binding, the thiolated probe structure ensures a uniform molecular coverage on the gold surface. These features of the hairpin probe minimizes the randomness of its molecular attachment to the NPGD substrate and, thus, increases the precision of molecular coverage on the 3-dimensional structure of NPGDs.

To prove this idea experimentally, different amounts (0–5 μL) of the ssDNA target sequence (40 nM) were mixed and hybridized with a fixed amount of the hairpin probe (5 μL, 40 nM) at 50 °C for 60 mins. With added phosphate buffer solution to a total 10 μL volume, the resulting concentrations (in nM) of hybridized dsDNA and unhybridized probe molecules in six samples were estimated to be (0,20), (4,20), (8,20), (12,20), (16,20), and (20,20). After cooling, 5 μL of each sample was dispensed onto the NPGD substrate surrounded by a polydimethylsiloxane (PDMS) well (2 mm diameter, 4 mm height) and allowed to incubate for 60 mins. The surface was then washed with deionized (DI) water and incubated in 0.1 mM mercapto-1-hexanol (MCH) for 30 mins to eliminate non-specific binding, followed by DI water rinse. In Figure 6A, the difference spectra are shown by subtracting the baseline

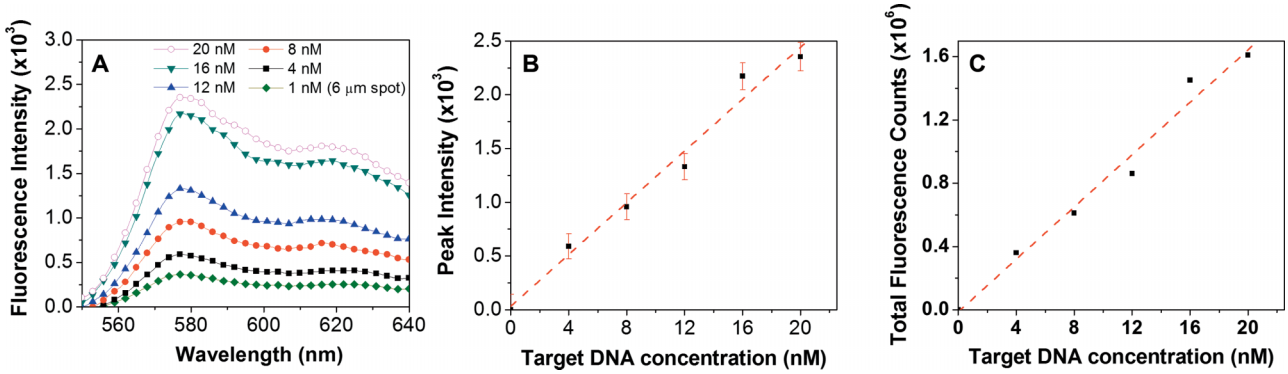

Figure 6 Fluorescence spectra, peak intensity, and total fluorescence counts: (**A**) With the probe signal used as reference baseline, the difference spectra at different target DNA concentration are plotted as labeled. Corresponding (**B**) peak intensity and (**C**) total intensity counts for each concentration step of the target DNA.

© 2015 by WILEY-VCH Verlag GmbH & Co. KGaA, Weinheim

spectrum (0 nM target) from others. We observe increased fluorescence as target concentration increased. In Figure 6B, the peak fluorescence intensity of the difference spectra are shown together with the error bars calculated from the average standard deviation across the entire spectral range. For example, at 4 nM, the peak intensity is ~500 counts and the error bar is ~120 counts, resulting in a peak-to-noise ratio of ~4. However, to fully utilize the signal output from the whole spectral range, we can consider the total fluorescence intensity to be the sum across the entire spectrum, and the error bar as the square root of the sum of variance across the entire spectrum. For example, at 4 nM, the total fluorescence intensity is ~500,000 counts with an error bar ~4060 counts, resulting in a signal-to-noise ratio (SNR) ~123. We estimate the amounts of dsDNA molecules to be ~2.4 zeptomole based on the laser spot size and the surface density calculation. More details on this quantification are provided in Supporting Information. In principle, the ultimate LOD in quantity is ~0.06 zeptomole for SNR~3.

3.5 Area-dependent concentration detection limit

Once the LOD in quantity is determined, we next determine the LOD in concentration, which depends on the measurement spot size. In other words, more fluorescence can be acquired from a larger spot with more molecules even at the same concentration.

Therefore, lower concentration LOD beyond 4 nM can be achieved by collecting fluorescence from a larger laser spot. Indeed, with a lower magnification objective (10X), the fluorescence spectrum (–◆–) in Figure 6A acquired from a 6 μm laser spot of a 1 nM dsDNA sample appears to be ~60% to that from a 4 nM sample with a 1.5 μm spot. The quantity of dsDNA within the 6 μm spot is ~4.2 zeptomole. Based on the SNR~60, the ultimate LOD in concentration can be much lower than 1 nM when a larger laser spot is employed. Furthermore, the concentration LOD is fundamentally limited by the binding efficiency of target molecules. Therefore, we would not provide any estimate based on the SNR. Nevertheless, a future direction appears to be implementing efficient means for bringing target molecules to the NPGD surface via physical manipulations such as dielectrophoresis [48]. In this work, none of the results required multivariate computational techniques, which are known to be highly effective to extract hidden spectroscopic information at low SNR [49–52].

In addition, there are certain features to the hairpin-based quench-enhancement mechanism that dictates the detection limit of the SEF sensor. The enhancement is highly dependent on the structural state of the hairpin DNA on the surface of the NPGD substrate. Subsequent increase in the total fluorescence is the result of the introduction of the molecular population that were effectively enhanced after hybridization. Since we are only measuring the ensemble average of the enhanced population over the laser spot, the detection limit can be only be estimated according to the expected coverage at a given target concentration. The statistical limitation of the signal averaging of the enhanced molecules deters single-molecule detection, and, hence, this is considered essential for future work with SEF on NPGD.

Furthermore, the results can be viewed in the context of Peng's results [47], which reported a concentration LOD of 500 pM in a microfluidic environment. We have analyzed their published protocol and data and estimated the upper-limit LOD in quantity to be 720 attomole of ssDNA target, which is about 10^5 times more than ours. The detailed analysis is provided in Supporting Information. Of course, their LOD could have been lower than 720 attomole depending on the actual fraction of probes that effectively hybridized.

4. Conclusions

We have developed a label-free sensing mechanism based on the distance-dependence of surface-enhanced fluorescence (SEF) due to conformational differences in DNA molecules on plasmonic nanoporous gold disks. Specifically, we have demonstrated the detection of 2.4 zeptomole quantity of ERBB2 DNA target on NPGD substrates, and showed the upper concentration detection limit of 1 nM. Nevertheless, based on the signal-to-noise ratio, an ultimate LOD in quantity of ~0.06 zeptomole is envisioned. To characterize the combined fluorescence enhancement and quenching on NPGD substrates, we have studied the effect of surface density of the fluorescent molecules without molecular spacers for the first time. We have demonstrated that NPGD substrates provide more effective SEF for both NIR and visible fluorophores compared to flat gold film and nonporous gold disks due to its high density plasmonic hot spots. A net fluorescence gain ~50 times compared to glass substrate has been achieved on NPGD substrates without molecular spacers, suggesting a potentially SEF factor higher than 50.

While the aim of the study is to introduce NPGDs as a novel SEF platform, further optimization can be achieved in future works by fine-tuning the physical parameters of the NPGDs (such as particle size, pore dimensions, substrate material) in order to further improve sensitivity. With a straightforward detection mechanism, the NGPDs can be con-

© 2015 by WILEY-VCH Verlag GmbH & Co. KGaA, Weinheim

veniently integrated into biochip and microfluidic devices for DNA sensing without the need for amplification techniques such as polymerase-chain reaction (PCR). With the aid of high sensitivity and target specificity, the NPGD sensing platforms have a high potential for applications in point-of-care biomarker detection.

Supporting information

Additional supporting information may be found in the online version of this article at the publisher's website: NPGD SEM Images, DNA target density estimation, and Estimation of probe molecular density for a microfluidic SEF sensor.

Acknowledgements W.C.S. acknowledges funding from the National Science Foundation (NSF) CAREER Award (CBET-1151154), the National Aeronautics and Space Administration (NASA) Early Career Faculty Grant (NNX12AQ44G), the Gulf of Mexico Research Initiative (GoMRI-030) and the Cullen College of Engineering at the University of Houston. We greatly appreciate Prof. Richard Willson of University of Houston for providing the DNA target and probes.

Author biographies Please see Supporting Information online.

References

[1] C. Tansakul, E. Lilie, E. D. Walter, F. Rivera, A. Wolcott, J. Z. Zhang, G. L. Millhauser, and R. Braslau, J. Phys. Chem. C **114**, 7793–7805 (2010).
[2] F. Lin, D. Pei, W. He, Z. Huang, Y. Huang, and X. Guo, J. Mater. Chem. **22**, 11801–11807 (2012).
[3] Z. Weihua, D. Fei, L. Wen-Di, W. Yuxuan, H. Jonathan, and Y. C. Stephen, Nanotechnology **23**, 225301 (2012).
[4] L. M. Freeman, S. Li, Y. Dayani, H.-S. Choi, N. Malmstadt, and A. M. Armani, Appl. Phys. Lett. **98**, 1437031–1437033 (2011).
[5] D. Yan, S. Qin, L. Chen, J. Lu, J. Ma, M. Wei, D. G. Evans, and X. Duan, Chem. Commun. (Cambridge, U. K.) **46**, 8654–8656 (2010).
[6] N. Ganesh, W. Zhang, P. C. Mathias, E. Chow, J. A. N. T. Soares, V. Malyarchuk, A. D. Smith, and B. T. Cunningham, Nat Nano **2**, 515–520 (2007).
[7] P. C. Mathias, H.-Y. Wu, and B. T. Cunningham, Appl. Phys. Lett. **95**, 21111 (2009).
[8] S. J. Norton and V.-D. Tuan, Nanotechnology, IEEE Transactions on **10**, 1264–1274 (2011).
[9] R. W. Johnson and T. Vo Dinh, Anal. Chem. **61**, 2766–2769 (1989).
[10] G. Manas Ranjan, H. Austin, S. Mayandi, C. Yi, and G. L. Liu, Nanotechnology **22**, 365203 (2011).
[11] T. Ming, H. Chen, R. Jiang, Q. Li, and J. Wang, J. Phys. Chem. Lett. **3**, 191–202 (2011).
[12] C. Geddes, A. Parfenov, D. Roll, I. Gryczynski, J. Malicka, and J. Lakowicz, J. Fluoresc. **13**, 267–276 (2003).
[13] Y. Chen, K. Munechika, and D. S. Ginger, Nano Lett. **7**, 690–696 (2007).
[14] M. Ranjan Gartia, J. P. Eichorst, R. M. Clegg, and G. Logan Liu, Appl. Phys. Lett. **101**, 0231181–0231185 (2012).
[15] J. R. Lakowicz, Y. Shen, S. D'Auria, J. Malicka, J. Fang, Z. Gryczynski, and I. Gryczynski, Anal. Biochem. **301**, 261–277 (2002).
[16] F. Emmanuel and G. S. Samuel, J. Phys. D: Appl. Phys. **41**, 013001 (2008).
[17] A. Wittstock, V. Zielasek, J. Biener, C. M. Friend, and M. Bäumer, Science **327**, 319–322.
[18] S. O. Kucheyev, J. R. Hayes, J. Biener, T. Huser, C. E. Talley, and A. V. Hamza, Appl. Phys. Lett. **89**, 053102–053103 (2006).
[19] Y. Yang, Y. Xia, W. Huang, J. Zheng, and Z. Li, J. Solid State Electrochem. **16**, 1733–1739 (2012).
[20] J. Biener, G. W. Nyce, A. M. Hodge, M. M. Biener, A. V. Hamza, and S. A. Maier, Adv. Mater. (Weinheim, Ger.) **20**, 1211–1217 (2008).
[21] X. Lang, L. Qian, P. Guan, J. Zi, and M. Chen, Appl. Phys. Lett. **98**, 093701–093703 (2011).
[22] F. Zhao, J. Zeng, M. M. Parvez Arnob, P. Sun, J. Qi, P. Motwani, M. Gheewala, C.-H. Li, A. Paterson, U. Strych, B. Raja, R. C. Willson, J. C. Wolfe, T. R. Lee, and W.-C. Shih, Nanoscale **6**, 8199–8207 (2014).
[23] J. Qi, P. Motwani, M. Gheewala, C. Brennan, J. C. Wolfe, and W.-C. Shih, Nanoscale **5**, 4105–4109 (2013).
[24] J. Zeng, F. Zhao, J. Qi, Y. Li, C.-H. Li, Y. Yao, T. R. Lee, and W.-C. Shih, RSC Adv. **4**, 36682–36688 (2014).
[25] M. M. P. Arnob, F. Zhao, J. Zeng, G. Santos, M. Li, and W.-C. Shih, Nanoscale **6**, 12470–12475 (2014).
[26] G. M. Santos, F. Zhao, J. Zeng, and W.-C. Shih, Nanoscale **6**, 5718–5724 (2014).
[27] J. Qi, J. Zeng, F. Zhao, S. H. Lin, B. Raja, U. Strych, R. C. Willson, and W.-C. Shih, Nanoscale **6**, 8521–8526 (2014).
[28] M. Li, J. Lu, J. Qi, F. Zhao, J. Zeng, J. C.-C. Yu, and W.-C. Shih, J. Biomed. Opt. **19**, 050501–050501 (2014).
[29] M. Li, F. Zhao, J. Zeng, J. Qi, J. Lu, and W.-C. Shih, J. Biomed. Opt. **19**, 111611–111611 (2014).
[30] A. Campion, A. R. Gallo, C. B. Harris, H. J. Robota, and P. M. Whitmore, Chem. Phys. Lett. **73**, 447–450 (1980).
[31] P. Anger, P. Bharadwaj, and L. Novotny, Phys. Rev. Lett. **96**, 113002 (2006).
[32] X. Y. Lang, P. F. Guan, T. Fujita, and M. W. Chen, Phys. Chem. Chem. Phys. **13**, 3795–3799 (2011).
[33] X. Y. Lang, P. F. Guan, L. Zhang, T. Fujita, and M. W. Chen, Appl. Phys. Lett. **96**, 073701 (2010).
[34] B. J. Dodgson, A. Mazouchi, D. W. Wegman, C. C. Gradinaru, and S. N. Krylov, Anal. Chem. **84**, 5470–5474 (2012).

© 2015 by WILEY-VCH Verlag GmbH & Co. KGaA, Weinheim

[35] G. Nöll, Q. Su, B. Heidel, and Y. Yu, Adv. Healthcare Mater. **3**, 42–46 (2014).
[36] B. Cannon, A. R. Campos, Z. Lewitz, K. A. Willets, and R. Russell, Anal. Biochem. **431**, 40–47 (2012).
[37] J. Qi and W.-C. Shih, Appl. Opt. **53**, 2881–2885 (2014).
[38] J. Qi and W.-C. Shih, Opt. Lett. **37**, 1289–1291 (2012).
[39] J. Qi, J. Li, and W.-C. Shih, Biomed. Opt. Express **4**, 2376–2382 (2013).
[40] K. Ray and J. R. Lakowicz, J. Phys. Chem. C **117**, 15790–15797 (2013).
[41] D. Pristinski, S. Tan, M. Erol, H. Du, and S. Sukhishvili, J. Raman Spectrosc. **37**, 762–770 (2006).
[42] P. Hildebrandt and M. Stockburger, J. Phys. Chem. **88**, 5935–5944 (1984).
[43] A. I. Dragan and C. D. Geddes, Appl. Phys. Lett. **100**, 093115 (2012).
[44] G. Hong, S. M. Tabakman, K. Welsher, Z. Chen, J. T. Robinson, H. Wang, B. Zhang, and H. Dai, Angew. Chem. Int. Ed. **50**, 4644–4648 (2011).
[45] Y. D. Yin and X. S. Zhao, Acc. Chem. Res. **44**, 1172–1181 (2011).
[46] A. Sassolas, B. D. Leca-Bouvier, and L. J. Blum, Chem. Rev. **108**, 109–139 (2008).
[47] H.-I. Peng, C. M. Strohsahl, and B. L. Miller, Lab Chip **12**, 1089–1093 (2012).
[48] A. Barik, L. M. Otto, D. Yoo, J. Jose, T. W. Johnson, and S.-H. Oh, Nano Lett. **14**, 2006–2012 (2014).
[49] W.-C. Shih, K. L. Bechtel, and M. S. Feld, Anal. Chem. **79**, 234–239 (2006).
[50] K. L. Bechtel, W.-C. Shih, and M. S. Feld, Opt. Express **16**, 12737–12745 (2008).
[51] W.-C. Shih, K. L. Bechtel, and M. S. Feld, Opt. Express **16**, 12726–12736 (2008).
[52] O. R. Šćepanović, K. L. Bechtel, A. S. Haka, W.-C. Shih, T.-W. Koo, A. J. Berger, and M. S. Feld, J. Biomed. Opt. **12**, 064012–064010 (2007).

© 2015 by WILEY-VCH Verlag GmbH & Co. KGaA, Weinheim